A global climatology of surface anticyclones, their variability, associated drivers and long-term trends

Acacia Pepler, Andrew Dowdy and Pandora Hope

Australian Bureau of Meteorology, Melbourne, Australia

Corresponding Author: Acacia Pepler. Email: acacia.pepler@bom.gov.au

Keywords: high pressure, anticyclone, blocking, reanalysis, climate variability, trends

This is a post-peer-review, pre-copyedit version of an article published in Climate Dynamics. The final authenticated version is available online at: https://doi.org/10.1007/s00382-018-4451-5

ABSTRACT

A global climatology of anticyclones identified at mean sea level pressure is presented based on multiple reanalyses over the period 1960–2016, including assessment of regional and seasonal variations, interannual variability, and long-term trends. Interannual variability is associated with the El Niño-Southern Oscillation (ENSO), particularly in the Pacific region during November–April. Anticyclones vary in phase with the strength and intensity of the local mean subtropical ridge, with anticyclone variability also associated with the Southern Annular Mode (SAM) in the Southern Hemisphere and the Arctic Oscillation (AO) in parts of the Northern Hemisphere, particularly during the cooler months of the year. Long-term climatological trends in anticyclone occurrence are presented, including back to 1960 using 20CR reanalysis data. The strongest trends occur in the Southern Hemisphere, including increases in anticyclone frequency in the latitudes 30-40 S and decreases for adjacent latitudes in both seasons, which can be partially attributed to changes in SAM during November-April.

1. INTRODUCTION

The climate of the global midlatitudes can be characterised by the passage of cyclones and anticyclones. While the impacts of cyclones on surface weather have been broadly studied, anticyclones can also cause significant impacts on surface weather. Anticyclones bring clear skies and descending air, and are thus associated with hot, dry days and cold nights, with slow-moving or stationary blocking highs capable of causing both heatwaves and cold outbreaks (Marshall et al. 2013; Gibson et al. 2017; Ioannidou and Yau 2008; Hatzaki et al. 2014). The interaction between surface cyclones and adjacent high pressure systems can also contribute to heavy rain in parts of the globe such as eastern Australia (Mills et al. 2010).

Numerous studies have investigated changes and variability in the frequency and characteristics of extratropical cyclones using a range of automated methods (Hodges et al. 2011; Simmonds and Keay 2000; Neu et al. 2013; Wang et al. 2013; Reboita et al. 2015; Leckebusch and Ulbrich 2004; Jones and Simmonds 1993; Raible et al. 2008; Pfahl and Wernli 2012). In comparison to cyclones, fewer studies have applied similar methods to investigate surface anticyclones. There have been no global studies of surface anticyclones, although hemispheric climatologies have been produced by Ioannidou and Yau (2008) for winter in the Northern Hemisphere (NH), and by Jones and Simmonds (1994) and Sinclair (1996) for the Southern Hemisphere (SH). There have been no climatologies of the NH surface anticyclones for seasons other than boreal winter, although there have been a number of in-depth regional studies in the NH, particularly in the Mediterranean (Hatzaki et al. (2014), and references therein).

To date, most studies have focussed on anticyclones in the upper atmosphere, with a global climatology of persistent maxima of 500 hPa geopotential height recently published by Liu et al. (2017). The special case of stationary "blocking" highs in the upper atmosphere has been extensively studied (Wiedenmann et al. 2002; Shakina and Ivanova 2010; Small et al. 2014; Croci-Maspoli et al. 2007; Barnes et al. 2014), but this focus on upper atmosphere blocking excludes the mobile high pressure systems that form the mid-latitude subtropical

ridges. No studies to date have assessed the sensitivity of trends in surface anticyclone behaviour to the choice of reanalysis. For this reason, there is a need for a global climatology of surface anticyclones, including an assessment of seasonal and interannual variability and long-term trends.

In the absence of global studies on anticyclones, there remains relatively little information on how these systems and their impacts are influenced by the main drivers of climate variability, such as the El Niño-Southern Oscillation, as well as long-term trends. In the Southern Hemisphere, relationships have previously been identified between anticyclones and climate indices such as the Southern Oscillation Index (SOI) and Pacific Decadal Oscillation (PDO) (Pezza and Ambrizzi 2003; Jones and Simmonds 1994). A decrease in the density of SH anticyclones during both the summer and winter seasons was identified in the ERA40 reanalysis between 1958 and 2002 (Pezza et al. 2007). Although similar studies do not exist for NH surface anticyclones, the positive phase of the Arctic Oscillation has been associated with an equatorward shift in the latitude of blocking highs in the Northern Hemisphere (Hassanzadeh and Kuang 2015). No consistent change in blocking frequency was observed between 1980 and 2012 for the NH (Barnes et al. 2014).

In this study, we will use a range of reanalyses to provide a global climatology of surface anticyclone activity, as well as assessing observed trends and interannual variability and their relationships with key climate drivers. Section 2 outlines the data and methods used, with section 3 providing a climatology of anticyclones across the globe, including how this varies between reanalyses. In section 4 we use the ERA-Interim reanalysis to assess the relationship between anticyclones and the drivers of interannual climate variability between 1980 and 2016. Section 5 uses ERAI as well as the longer NCEP and 20CR reanalyses to assess long-term trends, including the extent to which observed latitudinal trends can be attributed to changes in climate drivers including the Southern Annular Mode and Arctic Oscillation. Results are discussed in section 6.

2. METHODS

2.1 ANTICYCLONE TRACKING

Anticyclones are identified from gridded mean sea level pressure (SLP) data using the University of Melbourne cyclone detection and tracking scheme (Murray and Simmonds 1991; Simmonds et al. 1999). This method has been widely used for tracking both cyclones and anticyclones, particularly in the Southern Hemisphere (Pinto et al. 2005; Pepler et al. 2017; Lim and Simmonds 2002; Allen et al. 2010; Grieger et al. 2014; Pezza et al. 2007).

The tracking scheme has several steps. First, SLP from each reanalysis is regridded to a polar stereographic grid for each hemisphere, with an effective resolution of 1.5° at 30°S. Diffusive smoothing of the SLP data and a supplied topography file help to minimize erroneous highs associated with the reduction of pressure to mean sea level, with anticyclones masked above 1000km. This is consistent with how the same tracking scheme has been applied to low pressure systems (e.g. Simmonds and Keay 2000), as anticyclones or cyclones identified directly from MSLP show "bullseye"-type frequency anomalies in areas of elevated topography.

Anticyclones are identified as local minima in the Laplacian of SLP, with the average Laplacian of an anticyclone required to be below -0.075 hPa $(\text{deg.lat})^{-2}$ within a 10° radius of an anticyclone centre. An iterative technique

is then employed to identify a corresponding pressure maximum from a spline-fitted pressure field. Systems are tracked at a six-hourly resolution and grouped into events using a probability matching function. Events are required to persist for at least two instances (i.e. six hours), and the distance between the first and final observation of an anticyclone is required to be at least 500 km, consistent with Pezza et al. (2003, 2007). This has little impact on the spatial patterns of frequency or variability and predominantly removed very short-lived events, but removes bullseyes in areas where stationary systems are frequent and may be an artefact of the tracking procedure.

Systems are identified and tracked over several reanalyses, summarized in Table 1. The ERA-Interim reanalysis (ERAI) is one of the most widely used of the satellite-era reanalyses, and has been previously shown to be the most successful reanalysis at simulating cyclones in eastern Australia in comparison to satellite data (Pepler et al. 2018). Reanalyses that span a longer time period include the NCEP-NCAR reanalysis (NCEP1) and the 20th Century Reanalysis v2c ensemble (20CR). NCEP1 has data available from 1948, but it has been identified as having inhomogeneities at the start of the satellite era (Timbal and Hope 2008; Wang et al. 2016) as well as including some flaws in data assimilation over the Southern Ocean[1]. The 20th Century Reanalysis v2c ensemble (20CR) does not include these errors as it only assimilates station pressure observations, and additionally uses a 56-member ensemble, allowing assessment of the uncertainty in the reanalysis. The 20CR ensemble has been shown to have skill at identifying cyclones in the Australian region back to the early 20th century (Wang et al. 2013; Pepler et al. 2017), although trends are weaker than the similar ERA20C reanalysis (Wang et al. 2016). When using 20CR, in all cases anticyclone tracking is performed for each member separately and results are shown for either the full ensemble or the mean of the 56 members. The 20CR "Ensemble mean" pressure field is not used in this paper, as averaging the pressure field results in a smoother field that does not adequately represent cyclones or anticyclones (Pepler et al. 2017).

The paper focuses on the total number of anticyclones identified rather than the number of anticyclone events (tracks), due to the potential for uncertainty due to splitting of tracks, particularly when a high pressure system has multiple centres identified. As well as anticyclone frequency, we also assess key characteristics such as their duration, movement, radius and intensity. Anticyclone intensity is assessed using three metrics: the magnitude of the central pressure (hPa), the average Laplacian of pressure within a 10° radius of the anticyclone centre (hPa $(deg.lat)^{-2}$, which is given as a magnitude (i.e. positive values) for ease of interpretation), and the difference between the central pressure and the average pressure at the edge of the anticyclone (hPa). While this is technically the "height" of the anticyclone, we will refer to this as depth for consistency with papers that investigate the same metric for cyclones. The radius of the anticyclone is calculated as per Simmonds and Keay (2000), with the tracking scheme first identifying the anticyclone region as a polygon bound by the points where the Laplacian of pressure is equal to zero, before then calculating the (effective) radius of a circle with the same area.

[1]http://www.cpc.ncep.noaa.gov/products/wesley/paobs/paobs_1.html

For comparison of anticyclone characteristics between reanalyses and identifying relationships with large-scale climate drivers, we split analysis into two half-year periods, May-October and November-April. These correspond to the "cool" and "warm" seasons for the Southern Hemisphere ("warm" and "cool" in the Northern Hemisphere). Some results are also shown for the mid-latitude four meteorological seasons (March-May, MAM; June-August, JJA; September-November, SON; and December-February, DJF).

All post-processing and figure generation was performed using the R programming language. Statistical significance of trends and correlations are tested using a two-sided Student's t-test for $p<0.05$. To account for the problem of field significance and avoid overstating results, p values in spatial plots are adjusted using the False Discovery Rate method (Benjamini and Hochberg 1995; Wilks 2016).

2.2 Timeseries of large-scale climate drivers

We will assess the relationship between interannual variability in anticyclones and a number of indices of global atmospheric and oceanic variability.

The El Niño-Southern Oscillation (ENSO) is indicated by the Troup (1967) Southern Oscillation Index, available from the Bureau of Meteorology (http://www.bom.gov.au/climate/current/soihtm1.shtml). Another index of ENSO, SSTs in the NINO3.4 region, as well as the Dipole Mode Index (DMI), and index of Indian Ocean Dipole variability were retrieved from the NOAA Climate Prediction Centre (NOAA CPC; http://www.cpc.ncep.noaa.gov/). The NINO3.4 and DMI indices were calculated from Reynolds et al. (2002) weekly sea surface temperatures and converted to monthly index values by averaging the weekly values weighted by the number of days in the month.

NOAA CPC also provided indices of the Southern Annular Mode (SAM; listed as Antarctic Oscillation AOI), Arctic Oscillation (AOI), and North Atlantic Oscillation (NAO) from 1979 to 2016. This was supplemented by the station-based (Marshall 2003) SAM index for assessing the contribution of SAM to trends prior to 1979. Finally, the latitude of the edge of the Hadley Cell in the Northern and Southern Hemispheres were calculated from ERA-Interim reanalysis data by Nguyen et al. (2013) (provided by Nguyen, pers. comm. 2017). The Interdecadal Pacific Oscillation (IPO) tripole index was calculated from ERSST5 as per Henley et al. (2015) and is available at https://www.esrl.noaa.gov/psd/data/timeseries/IPOTPI/.

The position (STRP) and intensity (STRI) of the subtropical ridge (STR) are calculated for each hemisphere from both ERAI and the 20CR ensemble mean following the method of Drosdowsky (2005), with the STR for each longitude located based on a moving average window of 4° for 20CR and 3° for ERAI. Distinct from synoptic-scale ridges, which are not the focus of this paper, the monthly mean STRP indicates the latitude of the belt of high pressure in the subtropics. The STR is typically located at latitudes between 25-40°, and is weaker and further poleward during the summer months (e.g. Timbal and Drosdowsky 2013). In both hemispheres, a positive STR position refers to a poleward movement (higher latitude).

3. CLIMATOLOGY OF GLOBAL ANTICYCLONES

The average frequency of anticyclones during the period shared by all datasets (1980-2014) is shown in Figure 1 for all three reanalyses for the two halves of the year, with anticyclone frequency in the four meteorological seasons for ERAI shown in Figure 2. The three different reanalysis datasets show broad consistency with each other for the spatial variations in anticyclone frequency. The distribution of anticyclones in the Southern Hemisphere is consistent with Jones and Simmonds (1993) which used an earlier version of the same tracking scheme on operational Bureau of Meteorology pressure analyses. There is a strong belt of anticyclones between 30 and 50°S, with highest frequencies to the south of Australia and in the southwest of each ocean basin in all seasons, as well as high frequencies in the Tasman Sea east of Australia during the austral warm season (November-April).

In the NH there are similar belts of anticyclones over the North Atlantic and North Pacific basins, although the eastward extent in the Pacific varies by season, with anticyclones evident close to the North American coast in boreal winter (DJF). Over the continents there are anticyclones over Europe and North America, with fewer in summer (JJA). The belt of high pressure systems is less well-defined in the NH compared to the SH, with non-zero anticyclone frequencies at latitudes well into the Arctic, in agreement with other studies. This is the case across all seasons. Compared to the tracks of cyclones (Neu et al. 2013), anticyclones are typically located closer to the equator, particularly in the Southern Hemisphere where anticyclones are not observed in the main Southern Ocean storm track. The bands of high anticyclone activity are also more zonally oriented than observed for cyclones, which tend to have a stronger poleward component of movement.

Topographic filtering in the tracking scheme means that no anticyclone centres are identified over areas of elevated topography in parts of Asia and western North America. In comparison to Ioannidou and Yau (2008), there are similar spatial patterns of anticyclone frequency over North America in DJF, with a band of high frequency extending NW-SE over the inland US and an area of enhanced frequency on the east coast (Figure 2); however, we do not see the same area of enhanced anticyclone activity over Siberia. This is likely related to a combination of the use of topographic filtering as well as the different tracking schemes, as figures in Ioannidou and Yau (2008) show only anticyclones identified from high MSLP anomalies rather than anticyclonic vorticity so may also include areas of ridging.

The lower resolution reanalyses show some longitudinal variability in the anticyclone tracks, which is likely an artefact resulting from the conversion of lower resolution source grids onto the polar stereographic grid. When the anticyclone datasets were spatially smoothed using a 5° averaging window, the gridpoint correlations between interannual variability in the lower resolution reanalyses and ERA-Interim are higher than 0.8 across most of the globe. Correlations are weaker in areas with low average frequencies and in parts of the south Atlantic, southeast Pacific, and northeast North America, although these are still statistically significant.

Globally, the three reanalyses produce similar numbers of anticyclones, with similar characteristics (Table 2). On average, NCEP1 identifies more anticyclone events but of shorter average duration, while ERAI has the highest overall anticyclone frequency. Anticyclones in NCEP1 also tend to be smaller and weaker than in the other two reanalyses. The three reanalyses show similar latitudinal patterns of anticyclone activity (Figure 3) with peak frequencies at 37°S and 38°N, while the highest central pressures are found closer to 41°S and 61°N. Similar latitudinal profiles were observed for the Southern Hemisphere by (Jones and Simmonds 1994), although that paper also identified high anticyclone frequencies close to 80°S, attributed to the Antarctic anticyclone which was present on most days; this anticyclone is also absent in our analyses due to the high elevation of the Antarctic ice sheet. In the Southern Hemisphere, the latitude of maximum frequency moves from 39°S in February and March to 33°S in July, consistent with the seasonal cycle in the latitude of the subtropical ridge. The seasonal variation is larger in the Northern Hemisphere, from 29°N in February to 43°N in August, although the peak is less well defined in this hemisphere.

Although the anticyclone tracks are more latitudinally constrained in the Southern Hemisphere than in the Northern Hemisphere the total numbers of anticyclones are broadly similar in each hemisphere (Table 3). However, anticyclones in the Southern Hemisphere persist for 13-25 hours longer. This may be a consequence of the increased effect of topography on the tracking process in the NH, as anticyclone tracks are forced to terminate where they reach an area where anticyclones are not tracked due to high topography. The overall distance travelled by SH anticyclones is also larger, a combination of both the longer duration of anticyclones and a higher average movement speed. Anticyclones are generally stronger and more frequent during the local cool season, particularly in the Northern Hemisphere, while the average duration is longer during the local warm season (Table 3).

Southern Hemisphere anticyclones have higher intensities than their counterparts in the Northern Hemisphere when intensity is defined as the Laplacian or depth of the anticyclone, but central pressures 2-4 hPa lower. The higher pressures in the NH are mostly due to the large number of strong anticyclones at high latitudes in the NH, particularly during November-April, which are not observed in the Southern Hemisphere (Figures 3b, 4b). In the main anticyclone belts between 30 and 45°, the average central pressure is only 1 hPa higher in the NH, with broadly comparable pressure patterns (Figure 5). However, the pressure gradient poleward of the anticyclone centre is stronger in the SH, contributing to the higher average Laplacian of pressure.

Anticyclone radii are also larger in the SH than the NH, with the largest anticyclones on average observed in the southeast Pacific and southern Indian Oceans (Figure 4c), while radii tend to be smaller over land globally. Anticyclones tend to move more slowly in the NH, particularly in the Arctic and in the northwest Pacific and Atlantic (Figure 4d). In these regions more than 40% of anticyclones move slower than 20 km/h, particularly during the warm season (May-October). This is consistent with previous studies, which found that blocking highs are most frequency over the northwest of North America and west of Europe (Liu et al. 2017). Anticyclones tend to be faster-moving over Australia and eastern North America, particularly during the local warm season, but

slow-moving highs are also common in the Tasman Sea west of New Zealand, where they can have significant impacts on local climate (Marshall et al. 2013).

4. INTERANNUAL VARIABILITY OF ANTICYCLONE ACTIVITY

In areas where anticyclones are common, there are significant positive correlations between anticyclone frequency and the local mean MSLP (Figure 6a,d), particularly during the cool season ($r>0.4$). This is not surprising: as anticyclones are regions of relatively high pressure, a high frequency of anticyclones would be expected to be associated with higher average pressure. However, assigning causation in this region might be more complex than first thought given that anticyclone numbers can be weakly or negatively correlated with seasonal mean pressure (where anticyclones are relatively less common e.g. closer to the equator).

Throughout the Southern Hemisphere, variability in anticyclones is strongly associated with the strength and latitude of the subtropical ridge. A positive (poleward) STRP is associated with a poleward shift in anticyclone location, while a stronger subtropical ridge is associated with a latitudinal contraction, with more anticyclones in the latitudes of highest frequency but decreases to both the north and south. The subtropical ridge is less strongly related to anticyclones in the Northern Hemisphere, but similar patterns are observed in the North Atlantic and North Pacific during the cool season (November-April), while the local STR intensity is also positively correlated with anticyclone frequency in parts of Europe.

As well as pressure-based metrics, anticyclone frequency can also be related to many of the major climate drivers. Figure 7 shows the correlations between global anticyclone variability in the ERAI reanalysis from 1980 to 2016 and five key indices of global climate variability, oriented from north to south, with correlations shown separately for the two half-years. Correlations are only shown where they are statistically significant ($p<0.05$) based on local data and where the average anticyclone frequency is greater than 0.1 centres $(\text{deg.lat.})^{-2}$, while black contours indicate statistically significant correlations after accounting for the false discovery rate.

The hemispheric belts of anticyclone activity are located equatorward of the main midlatitude storm tracks. Accordingly, just as the expansion and contraction of the midlatitude westerlies are associated with shifts in the average latitude of the storm track, they are also related to the average intensity and latitude of the subtropical ridge and associated anticyclone activity.

The Southern Annular Mode (SAM, also sometimes referred to as the Antarctic Oscillation) is a key extratropical climate driver in the Southern Hemisphere, with positive SAM conditions associated with a poleward contraction of the midlatitude storm track. Accordingly, positive SAM is associated with an increase in anticyclone frequency between 40-50°S in both seasons but particularly May-October, and a decrease in anticyclone frequency further north (Figure 7e,j). The influence of SAM on anticyclones is strongest in the southern Indian Ocean and the southwest Pacific, with a strong positive correlation in southern Argentina during May-October. In southeast Australia, positive SAM is associated with an increase in anticyclonicity during May-October but a decrease

during November-April, particularly during the austral spring and summer, consistent with the seasonal variation in correlations between SAM and rainfall in this region (Hendon et al. 2007).

In the Northern Hemisphere, both the Arctic Oscillation, the Northern Hemisphere counterpart of SAM, as well as the North Atlantic Oscillation (not shown) are strongly correlated with anticyclone frequency in the North Atlantic during November-April, with positive AOI associated with a poleward shift in anticyclones (Figure 7f). Positive AOI is also associated with an increase in anticyclone frequency over western Europe and decreases in parts of Russia. However, unlike in the Southern Hemisphere, there are no consistent correlations between AOI and Northern Hemisphere anticyclonicity during the warm season May-October (Figure 7a), with positive AOI associated with a poleward shift in Pacific anticyclones during boreal autumn but no change in the summer months.

During May-October, the latitudinal extent of the Hadley Cell has relatively little association with the location or frequency of global anticyclones, with the exception of parts of the southeast Pacific where a northward shift in the latitude of the edge of the Southern Hemisphere Hadley Cell is associated with a decrease in anticyclone frequency between 30-50°S (Figure 6b,d). In contrast, there are strong correlations between the edge of the Hadley Cell and anticyclone frequency in the Pacific during November-April, particularly over southern Australia, as well as a positive correlation between Hadley Cell latitude and anticyclone frequency in the northeast US and North Pacific (Figure 7g,i). The similar spatial structure of correlations (of opposing sign) between Figures 7g and 7i are explained by the strong negative correlations between the SH and NH Hadley cell extent during November-April (r=-0.61). Significant correlations are also observed between the SH latitude and SAM (r=-0.47) and between the NH latitude and AOI (+0.49) in November-April, while the Hadley Cell extent is independent of the other extratropical modes (i.e., SAM and AO) during May-October.

Anticyclone frequency is also associated with variability in the tropics, including the El Niño-Southern Oscillation (ENSO), the dominant mode of global variability at seasonal to interannual time scales. During November-April, the SOI is strongly correlated with the latitude of the Hadley Cell in both the Southern Hemisphere (r=-0.80) and Northern Hemisphere (r=+0.65). Consequently, El Niño (negative SOI) shows a similar pattern of correlations with Southern Hemisphere anticyclones as shown for changes in the latitude of the Hadley Cell (Figure 7h). The Henley et al. (2015) IPO index and NINO3.4 index have similar spatial correlation patterns (not shown).

During May-October, correlations between ENSO and anticyclones are restricted to parts of the southeast Pacific and southern Australia. While these correlations are not statistically significant when accounting for field significance, similar (and statistically significant) correlation patterns are observed for the same regions when using the longer 20CR and NCEP1 reanalyses. The area of negative correlations around southeast Australia is also observed for the DMI index, an indicator of the strength of the Indian Ocean Dipole (IOD, not shown). This spatial pattern is consistent with previous studies that identified IOD as playing a key role in the teleconnections between ENSO and southern Australian rainfall including through its impact on the midlatitude westerlies (Ummenhofer et al. 2009; Pepler et al. 2014; Cai et al. 2011).

5. Long-term trends in anticyclone frequency

Figure 8 shows the linear trend in anticyclone frequency for each half-year between 1980 and 2016 (2014 in the case of 20CR). Given the relatively short time period, trends across much of the globe are weak and non-significant across the three reanalyses; however, there are some areas of agreement. During May-October, the most significant trends are observed over Europe, with increases in anticyclone frequency over parts of Scandinavia and western Russia of more than 2% per year. Increases are also observed in parts of the Southern Hemisphere midlatitudes. Trends in November-April are less consistent, particularly in the Southern Hemisphere, but a dipole pattern can be observed in the north Pacific with a poleward shift in anticyclone occurrence and an increase in frequency in the Bering Strait.

Figure 9 shows the change in total anticyclone frequency between 1960-1979 and 1997-2016. This period was chosen to reflect the longer term trends while minimising inhomogeneities associated with changing data availability, particularly associated with the increase in data available after the 1957-1958 International Geophysical Year. Consistency between reanalyses is lower for this period, particularly in the Southern Ocean where observations are less frequent and where NCEP1 has known inhomogeneities between 1979 and 1992 (Timbal and Hope 2008; Wang et al. 2016). However, the decrease in anticyclones in this region in 20CR is consistent with the shorter-term trends in ERAI (Figure 8).

The most robust trends are observed in the Southern Hemisphere midlatitudes, with statistically significant increases in anticyclone frequency over parts of southern and eastern Australia in both reanalyses in recent decades, as well as an increase in the frequency of anticyclones off the Argentina coast during November-April. Changes are weaker and less consistent between the reanalyses in the Northern Hemisphere, including in the parts of the North Pacific which had strong trends in Figure 8, but a strong increase in November-April anticyclone frequency is also observed in the north Atlantic. The weaker trends in the Northern Hemisphere are consistent with previous work on blocking indices, with trends sensitive to region, reanalysis, blocking index and time period (Barnes et al. 2014; Croci-Maspoli et al. 2007; Small et al. 2014).

The latitudinal patterns of trends in anticyclone activity in the Southern Hemisphere are broadly consistent with the relationship between anticyclone frequency and the latitudinal width of both the tropics (represented by the Hadley Cell edge) and the extratropics (represented by SAM). Global climate models project a poleward expansion of the tropics and a positive trend in SAM, with a positive SAM trend in recent decades, particularly during the austral summer, attributed to a combination of greenhouse warming and ozone depletion (Arblaster et al. 2011; Grise et al. 2014; Thomas et al. 2015). This raises the question: to what extent can the observed trends in anticyclone activity be attributed to long-term changes in these indices?

Figure 10 shows the change in average anticyclone frequency between 1960-1979 and 1997-2016 by latitude for both the 20CR and NCEP reanalyses. Consistent with the spatial pattern of changes shown in Figure 9, as well

as the latitudinal distribution of anticyclones shown in Figure 3, there is a large increase in anticyclone frequency at latitudes 30-40°S during May-October, and between 35-45°S during November-April. In 20CR this is balanced by the decreased frequency in the Southern Ocean, with no statistically significant change in the total number of Southern Hemisphere or global anticyclones in either season. As NCEP1 does not produce a decline in Southern Ocean anticyclones, it has a statistically significant 4.7% increase in anticyclones globally, largest during November-April. The increase in frequency is concentrated at the centre of the mean anticyclone track rather than reflecting a shift in the location of anticyclones, with a 1° poleward shift in the latitude of peak occurrence in May-October but no robust change in November-April.

In addition, we show the change that is congruent with observed changes in the SAM and the hemispheric mean intensity of the subtropical ridge (STRI) over the same period. This is calculated by first linearly detrending the time series of both anticyclone frequency and the index values (of SAM and STRI). The detrended time series are used to calculate the linear regression coefficients of the relationship between anticyclone occurrence at a latitude and the index. The index is then multiplied by the regression coefficient and the mean frequency added, to create an artificial time series of the expected number of anticyclones relating to the index values alone. Finally, the change in this artificial timeseries is calculated to indicate the change that would be expected based on the observed changes in the index and the relationship between that index and anticyclone occurrence.

During the Southern Hemisphere warm season, November-April, close to half of the observed increase in anticyclone frequency can be attributed to the positive trend in SAM, which is associated with a poleward shift in the latitude of anticyclones (Figure 6). A similar proportion of the trend can be attributed to the observed intensification of the Southern Hemisphere subtropical ridge, which can also explain close to half of the observed increase in anticyclones during May-October, with correlations of ~ 0.4 between SAM and STRI in both seasons. As the Hadley Cell latitude was calculated from ERA-Interim, the data do not extend early enough to allow an assessment of how this measure is linked to the trends; however, the strongest increases in anticyclone activity are observed over southern Australia (Figure 8). Changes in the Southern Hemisphere Hadley Cell are not expected to provide additional explanatory power in this region due to the weak relationships shown in Figure 6d. The role of the Interdecadal Pacific Oscillation was also assessed but had little change between the periods in either season, with an annual average IPO of -0.25 in 1960-1979 and -0.16 in 1997-2016.

6. Conclusions

Numerous papers have investigated the frequency, variability and trends in global cyclone activity, including their sensitivity to the reanalyses and tracking methods used (Neu et al. 2013; Reboita et al. 2015; Wang et al. 2016). In comparison, anticyclones have received much less attention, despite their important impacts on severe weather events including heatwaves, droughts and cold extremes (Boschat et al. 2015; Marshall et al. 2013;

Gibson et al. 2017) and their potential links with long-term drying in parts of the global midlatitudes such as southern Australia (Timbal and Drosdowsky 2013) and southern Africa.

This paper presents the first global climatology of surface anticyclone activity, characteristics, variability and trends, using three reanalyses: ERA-Interim, NCEP1, and the 20th Century Reanalysis 56 member ensemble. Consistent with earlier studies, there is a strong belt of anticyclones between 25-50°S in the Southern Hemisphere, which is further north during the cool season and to the south during the warm season. Anticyclones are less latitudinally coherent in the Northern Hemisphere, with anticyclone tracks equatorward of the major storm tracks in the north Pacific and Atlantic, but anticyclones potentially forming well into the Arctic region. Anticyclones in the Southern Hemisphere are typically larger and more long-lived than their Northern Hemisphere counterparts, with stronger Laplacians and greater "depths", but have lower central pressures.

Unsurprisingly, global anticyclone frequency is strongly influenced by extratropical variability and large-scale circulation features. In the Southern Hemisphere, positive SAM is associated with a poleward shift in anticyclones, while the Arctic Oscillation has a similar impact on anticyclones in the North Atlantic. During November-April, the expansion of the Hadley Cell, as measured by the latitude of its edge, is also associated with changes in anticyclone frequency, with a poleward shift in the Hadley Cell edge associated with a poleward shift in anticyclones in both hemispheres, particularly in the Pacific. Hadley Cell expansion is strongly correlated with the SOI during November-April, so this expansion largely reflects the impact of ENSO on global anticyclone activity. This has also been previously shown for the Southern Hemisphere (Jones and Simmonds 1994; Pezza et al. 2007). ENSO is also associated with changes in anticyclone activity in the southwest Pacific and southeast Australia during May-October.

Between 1960-1979 and 1997-2014, there was a significant increase in anticyclone frequency across the Southern Hemisphere midlatitudes during both seasons, which is consistent between the NCEP and 20CR reanalyses. This trend is largest to the southeast of Australia, where large decreases in cool season rainfall have been observed, associated with an intensification of the subtropical ridge (Larsen and Nicholls 2009; Timbal and Drosdowsky 2013), as well as to the west of Argentina. Trends are less consistent during the shorter period 1980-2016, although an increasing trend is also noted south of Australia during May-October. In the Northern Hemisphere, there was a poleward shift of North Pacific anticyclones in November-April between 1980 and 2016, as well as a decrease in anticyclones over Europe and corresponding increase to the northeast in both seasons; however, these trends are less robust using the longer 1960 to 2014 period, so likely reflect internal decadal variability.

The increase in the frequency of anticyclones in the Southern Hemisphere midlatitudes can be partially attributed to the intensification of the subtropical ridge, with the positive trend in SAM also contributing to the increase in anticyclones during November-April. Both these trends have been previously linked with anthropogenic influences, including both greenhouse gases and changes in ozone (e.g. Thomas et al. 2015; Timbal and Drosdowsky 2013), suggesting that anthropogenic influences may also play a role in the observed

changes in anticyclone frequency. Consequently, future work will assess in more detail the drivers of this strong trend and the extent to which it is associated with past and future climate change.

Acknowledgements

This project is jointly funded by the Victorian Department of Environment, Land, Water and Planning and the Earth Systems and Climate Change Hub of the Australian Government's National Environmental Science Programme, and was assisted by resources from the Australian National Computational Infrastructure (NCI). The authors thank Linden Ashcroft, Kevin Keay, and two anonymous reviewers for their comments on earlier versions of the paper, and Hanh Nguyen for providing the Hadley Cell datasets. All datasets used are freely available from their respective agencies, and anticyclone data is available for research use by contacting the authors.

References

Allen, J. T., A. B. Pezza, and M. T. Black, 2010: Explosive cyclogenesis: A global climatology comparing multiple reanalyses. *J. Clim.*, **23**, 6468–6484, doi:10.1175/2010JCLI3437.1.

Arblaster, J. M., G. A. Meehl, and D. J. Karoly, 2011: Future climate change in the Southern Hemisphere: Competing effects of ozone and greenhouse gases. *Geophys. Res. Lett.*, **38**, L02701, doi:10.1029/2010GL045384.

Barnes, E. A., E. Dunn-Sigouin, G. Masato, and T. Woollings, 2014: Exploring recent trends in Northern Hemisphere blocking. *Geophys. Res. Lett.*, **41**, 638–644, doi:10.1002/2013GL058745.

Benjamini, Y., and Y. Hochberg, 1995: Controlling the False Discovery Rate: A Practical and Powerful Approach to Multiple Testing. *J. R. Stat. Soc. Ser. B*, **57**, 289–300.

Boschat, G., A. Pezza, I. Simmonds, S. Perkins, T. Cowan, and A. Purich, 2015: Large scale and sub-regional connections in the lead up to summer heat wave and extreme rainfall events in eastern Australia. *Clim. Dyn.*, **44**, 1823–1840, doi:10.1007/s00382-014-2214-5.

Cai, W., P. van Rensch, T. Cowan, and H. H. Hendon, 2011: Teleconnection Pathways of ENSO and the IOD and the Mechanisms for Impacts on Australian Rainfall. *J. Clim.*, **24**, 3910–3923, doi:10.1175/2011JCLI4129.1.

Compo, G. P., and Coauthors, 2011: The Twentieth Century Reanalysis Project. *Q. J. R. Meteorol. Soc.*, **137**, 1–28, doi:10.1002/qj.776.

Croci-Maspoli, M., C. Schwierz, and H. C. Davies, 2007: A multifaceted climatology of atmospheric blocking and its recent linear trend. *J. Clim.*, **20**, 633–649, doi:10.1175/JCLI4029.1.

Dee, D. P., and Coauthors, 2011: The ERA-Interim reanalysis: configuration and performance of the data assimilation system. *Q. J. R. Meteorol. Soc.*, **137**, 553–597, doi:10.1002/qj.828.

Drosdowsky, W., 2005: The latitude of the subtropical ridge over Eastern Australia: The L index revisited. *Int. J. Climatol.*, **25**, 1291–1299, doi:10.1002/joc.1196.

Gibson, P. B., A. J. Pitman, R. Lorenz, and S. E. Perkins-Kirkpatrick, 2017: The Role of Circulation and Land Surface

Conditions in Current and Future Australian Heat Waves. *J. Clim.*, **30**, 9933–9948, doi:10.1175/JCLI-D-17-0265.1.

Grieger, J., G. C. Leckebusch, M. G. Donat, M. Schuster, and U. Ulbrich, 2014: Southern Hemisphere winter cyclone activity under recent and future climate conditions in multi-model AOGCM simulations. *Int. J. Climatol.*, **34**, 3400–3416, doi:10.1002/joc.3917.

Grise, K. M., S. W. Son, G. J. P. Correa, and L. M. Polvani, 2014: The response of extratropical cyclones in the Southern Hemisphere to stratospheric ozone depletion in the 20th century. *Atmos. Sci. Lett.*, **15**, 29–36, doi:10.1002/asl2.458.

Hassanzadeh, P., and Z. Kuang, 2015: Blocking variability: Arctic Amplification versus Arctic Oscillation. *Geophys. Res. Lett.*, **42**, 8586–8595, doi:10.1002/2015GL065923.

Hatzaki, M., H. A. Flocas, I. Simmonds, J. Kouroutzoglou, K. Keay, and I. Rudeva, 2014: Seasonal aspects of an objective climatology of anticyclones affecting the mediterranean. *J. Clim.*, **27**, 9272–9289, doi:10.1175/JCLI-D-14-00186.1.

Hendon, H. H., D. W. J. Thompson, and M. C. Wheeler, 2007: Australian rainfall and surface temperature variations associated with the Southern Hemisphere annular mode. *J. Clim.*, **20**, 2452–2467, doi:10.1175/JCLI4134.1.

Henley, B. J., J. Gergis, D. J. Karoly, S. Power, J. Kennedy, and C. K. Folland, 2015: A Tripole Index for the Interdecadal Pacific Oscillation. *Clim. Dyn.*, **45**, 3077–3090, doi:10.1007/s00382-015-2525-1.

Hodges, K. I., R. W. Lee, and L. Bengtsson, 2011: A comparison of extratropical cyclones in recent reanalyses ERA-Interim, NASA MERRA, NCEP CFSR, and JRA-25. *J. Clim.*, **24**, 4888–4906, doi:10.1175/2011JCLI4097.1.

Ioannidou, L., and M. K. Yau, 2008: A climatology of the Northern Hemisphere winter anticyclones. *J. Geophys. Res. Atmos.*, **113**, D08119, doi:10.1029/2007JD008409.

Jones, D. A., and I. Simmonds, 1993: A climatology of Southern Hemisphere extratropical cyclones. *Clim. Dyn.*, **9**, 131–145, doi:10.1007/BF00209750.

Jones, D. A., and I. Simmonds, 1994: A climatology of Southern Hemisphere anticyclones. *Clim. Dyn.*, **10**, 333–348.

Kalnay, E., and Coauthors, 1996: The NCEP/NCAR 40-Year Reanalysis Project. *Bull. Am. Meteorol. Soc.*, **77**, 437–471, doi:10.1175/1520-0477(1996)077<0437:TNYRP>2.0.CO;2.

Larsen, S. H., and N. Nicholls, 2009: Southern Australian rainfall and the subtropical ridge: Variations interrelationships, and trends. *Geophys. Res. Lett.*, **36**, 1–5, doi:10.1029/2009GL037786.

Leckebusch, G. C., and U. Ulbrich, 2004: On the relationship between cyclones and extreme windstorm events over Europe under climate change. *Glob. Planet. Change*, **44**, 181–193, doi:10.1016/j.gloplacha.2004.06.011.

Lim, E.-P., and I. Simmonds, 2002: Explosive Cyclone Development in the Southern Hemisphere and a Comparison with Northern Hemisphere Events. *Mon. Weather Rev.*, **130**, 2188–2209, doi:10.1175/1520-0493(2002)130<2188:ECDITS>2.0.CO;2.

Liu, P., and Coauthors, 2017: Climatology of tracked persistent maxima of 500-hPa geopotential height. *Clim. Dyn.*, **0**, 1–17, doi:10.1007/s00382-017-3950-0.

Marshall, A. G., D. Hudson, M. C. Wheeler, O. Alves, H. H. Hendon, M. J. Pook, and J. S. Risbey, 2013: Intra-seasonal drivers of extreme heat over Australia in observations and POAMA-2. *Clim. Dyn.*, **43**, 1915–1937, doi:10.1007/s00382-013-2016-1.

Marshall, G. J., 2003: Trends in the Southern Annular Mode from observations and reanalyses. *J. Clim.*, **16**, 4134–4143, doi:10.1175/1520-0442(2003)016<4134:TITSAM>2.0.CO;2.

Mills, G. A., R. Webb, N. E. Davidson, J. Kepert, A. Seed, and A. D., 2010: *The Pasha Bulker east coast low of 8 June 2007*. pp. 74 pages pp.

Murray, R. J., and I. Simmonds, 1991: A numerical scheme for tracking cyclone centres from digital data. Part I: Development and operation of the scheme. *Aust. Meteorol. Mag.*, **39**, 155–166.

Neu, U., and Coauthors, 2013: Imilast: A community effort to intercompare extratropical cyclone detection and tracking algorithms. *Bull. Am. Meteorol. Soc.*, **94**, 529–547, doi:10.1175/BAMS-D-11-00154.1.

Nguyen, H., A. Evans, C. Lucas, I. Smith, and B. Timbal, 2013: The hadley circulation in reanalyses: Climatology, variability, and Change. *J. Clim.*, **26**, 3357–3376, doi:10.1175/JCLI-D-12-00224.1.

Pepler, A., B. Timbal, C. Rakich, and A. Coutts-Smith, 2014: Indian ocean dipole overrides ENSO's influence on cool season rainfall across the Eastern seaboard of Australia. *J. Clim.*, **27**, 3816–3826, doi:10.1175/JCLI-D-13-00554.1.

Pepler, A. S., J. Fong, and L. V. Alexander, 2017: Australian east coast mid-latitude cyclones in the 20th Century Reanalysis ensemble. *Int. J. Climatol.*, **37**, 2187–2192, doi:10.1002/joc.4812.

Pepler, A. S., A. Di Luca, and J. P. Evans, 2018: Independently assessing the representation of midlatitude cyclones in high-resolution reanalyses using satellite observed winds. *Int. J. Climatol.*, **38**, 1314–1327, doi:10.1002/joc.5245.

Pezza, A. B., and T. Ambrizzi, 2003: Variability of Southern Hemisphere cyclone and anticyclone behavior: Further analysis. *J. Clim.*, **16**, 1075–1083, doi:http://dx.doi.org/10.1175/1520-0442(2003)016<1075:VOSHCA>2.0.CO;2.

——, I. Simmonds, and J. A. Renwick, 2007: Southern Hemisphere cyclones and anticyclones: recent trends and links with decadal variability in the Pacific Ocean. *Int. J. Climatol.*, **27**, 1403–1419, doi:10.1002/joc.1477.

Pfahl, S., and H. Wernli, 2012: Quantifying the relevance of cyclones for precipitation extremes. *J. Clim.*, **25**, 6770–6780, doi:10.1175/JCLI-D-11-00705.1.

Pinto, J. G., T. Spangehl, U. Ulbrich, and P. Speth, 2005: Sensitivities of a cyclone detection and tracking algorithm: Individual tracks and climatology. *Meteorol. Zeitschrift*, **14**, 823–838, doi:10.1127/0941-2948/2005/0068.

Raible, C. C., P. M. Della-Marta, C. Schwierz, H. Wernli, and R. Blender, 2008: Northern Hemisphere Extratropical Cyclones: A Comparison of Detection and Tracking Methods and Different Reanalyses. *Mon. Weather Rev.*, **136**, 880–897, doi:10.1175/2007MWR2143.1.

Reboita, M. S., R. P. da Rocha, T. Ambrizzi, and C. D. Gouveia, 2015: Trend and teleconnection patterns in the climatology of extratropical cyclones over the Southern Hemisphere. *Clim. Dyn.*, **45**, 1929–1944, doi:10.1007/s00382-014-2447-3.

Reynolds, R. W., N. A. Rayner, T. M. Smith, D. C. Stokes, and W. Wang, 2002: An Improved In Situ and Satellite SST Analysis for Climate. *J. Clim.*, **15**, 1609–1625, doi:10.1175/1520-0442(2002)015<1609:AIISAS>2.0.CO;2.

Shakina, N. P., and A. R. Ivanova, 2010: The blocking anticyclones: the state of studies and forecasting. *Russ. Meteorol. Hydrol.*, **35**, 721–730, doi:10.3103/S1068373910110014.

Simmonds, I., and K. Keay, 2000: Mean Southern Hemisphere extratropical cyclone behavior in the 40-year NCEP-NCAR reanalysis. *J. Clim.*, **13**, 873–885, doi:10.1175/1520-0442(2000)013<0873:MSHECB>2.0.CO;2.

Simmonds, I., R. J. Murray, and R. M. Leighton, 1999: A refinement of cyclone tracking methods with data from FROST. *Aust. Meteorol. Mag.*, Spec Ed:35-49.

Sinclair, M. R., 1996: A climatology of anticyclones and blocking for the Southern Hemisphere. *Mon. Weather Rev.*, **124**, 245–263.

Small, D., E. Atallah, and J. R. Gyakum, 2014: An objectively determined blocking index and its Northern Hemisphere climatology. *J. Clim.*, **27**, 2948–2970, doi:10.1175/JCLI-D-13-00374.1.

Thomas, J. L., D. W. Waugh, and A. Gnanadesikan, 2015: Southern Hemisphere extratropical circulation: Recent trends and natural variability. *Geophys. Res. Lett.*, **42**, 2015GL064521, doi:10.1002/2015GL064521.

Timbal, B., and P. Hope, 2008: Observed Early Winter Mean Sea Level Pressure Changes over Southern Australia: a comparison of existing datasets. *CAWCR Res. Lett.*, **1**, 1–33.

Timbal, B., and W. Drosdowsky, 2013: The relationship between the decline of Southeastern Australian rainfall and the strengthening of the subtropical ridge. *Int. J. Climatol.*, **33**, 1021–1034, doi:10.1002/joc.3492.

Troup, A. J., 1967: Opposition of anomolies of upper tropospheric winds at Singapore and Canton Island. *Aust. Meteorol. Mag.*, **15**, 32–37.

Ummenhofer, C. C., M. H. England, P. C. McIntosh, G. A. Meyers, M. J. Pook, J. S. Risbey, A. Sen Gupta, and A. S. Taschetto, 2009: What causes southeast Australia's worst droughts? *Geophys. Res. Lett.*, **36**, L04706, doi:10.1029/2008GL036801.

Wang, X. L., Y. Feng, G. P. Compo, V. R. Swail, F. W. Zwiers, R. J. Allan, and P. D. Sardeshmukh, 2013: Trends and low frequency variability of extra-tropical cyclone activity in the ensemble of twentieth century reanalysis. *Clim. Dyn.*, **40**, 2775–2800, doi:10.1007/s00382-012-1450-9.

——, Y. Feng, R. Chan, and V. Isaac, 2016: Inter-comparison of extra-tropical cyclone activity in nine reanalysis datasets. *Atmos. Res.*, **181**, 133–153, doi:10.1016/j.atmosres.2016.06.010.

Wiedenmann, J. M., A. R. Lupo, I. I. Mokhov, and E. A. Tikhonova, 2002: The climatology of blocking anticyclones for the Northern and Southern Hemispheres: Block intensity as a diagnostic. *J. Clim.*, **15**, 3459–3473, doi:10.1175/1520-0442(2002)015<3459:TCOBAF>2.0.CO;2.

Wilks, D. S., 2016: "The Stippling Shows Statistically Significant Grid Points": How Research Results are Routinely Overstated and Overinterpreted, and What to Do about It. *Bull. Am. Meteorol. Soc.*, **97**, 2263–2273, doi:10.1175/BAMS-D-15-00267.1.

Tables:

Table 1. Reanalyses used in this study

Reanalysis	Period Covered	Resolution	Reference	Comment
20CR	1851-2014	2°	Compo et al. (2011)	56-member ensemble
ERAI	1979-2017	0.75°	Dee et al. (2011)	
NCEP1	1948-2017	2.5°	Kalnay et al. (1996)	

Table 2. Global average annual anticyclone statistics during the period 1980-2014. Results for 20CR are the mean across the 56 ensemble members.

	ERAI	NCEP1	20CR
Events	1267	1334	1266
Average duration (days)	2.9	2.5	2.7
Average movement (km)	1884	1636	1740
Total instances	15853	14570	14821
Average central pressure (hPa)	1027.2	1027.0	1027.4
Average Laplacian (hPa $(deg.lat)^{-2}$)	0.20	0.19	0.20
Average radius (degrees)	7.9	7.2	8.3
Average depth (hPa)	6.5	6.0	6.9

Table 3. Global average annual anticyclone statistics during the period 1980-2014 for the ERAI reanalysis by season and hemisphere.

	Southern Hemisphere				Northern Hemisphere			
	DJF	MAM	JJA	SON	DJF	MAM	JJA	SON
Events	153	155	165	164	187	167	109	168
Average duration (days)	3.3	3.5	3.2	3.3	2.2	2.5	2.6	2.5
Average movement (km)	2221	2372	2193	2239	1581	1552	1160	1642
Total instances	2192	2297	2290	2294	1838	1860	1257	1827
Average central pressure (hPa)	1023.7	1025.7	1027.7	1026.3	1031.7	1029.5	1025.6	1028.4
Average Laplacian	0.20	0.22	0.22	0.21	0.20	0.19	0.15	0.19
Average radius (degrees)	8.4	8.4	8.5	8.5	6.9	7.2	7.2	7.0
Average depth (hPa)	6.4	7.1	7.3	6.9	6.4	6.2	5.1	6.2
Peak latitude	38	38	33	34	32	35	41	41

List of Figures

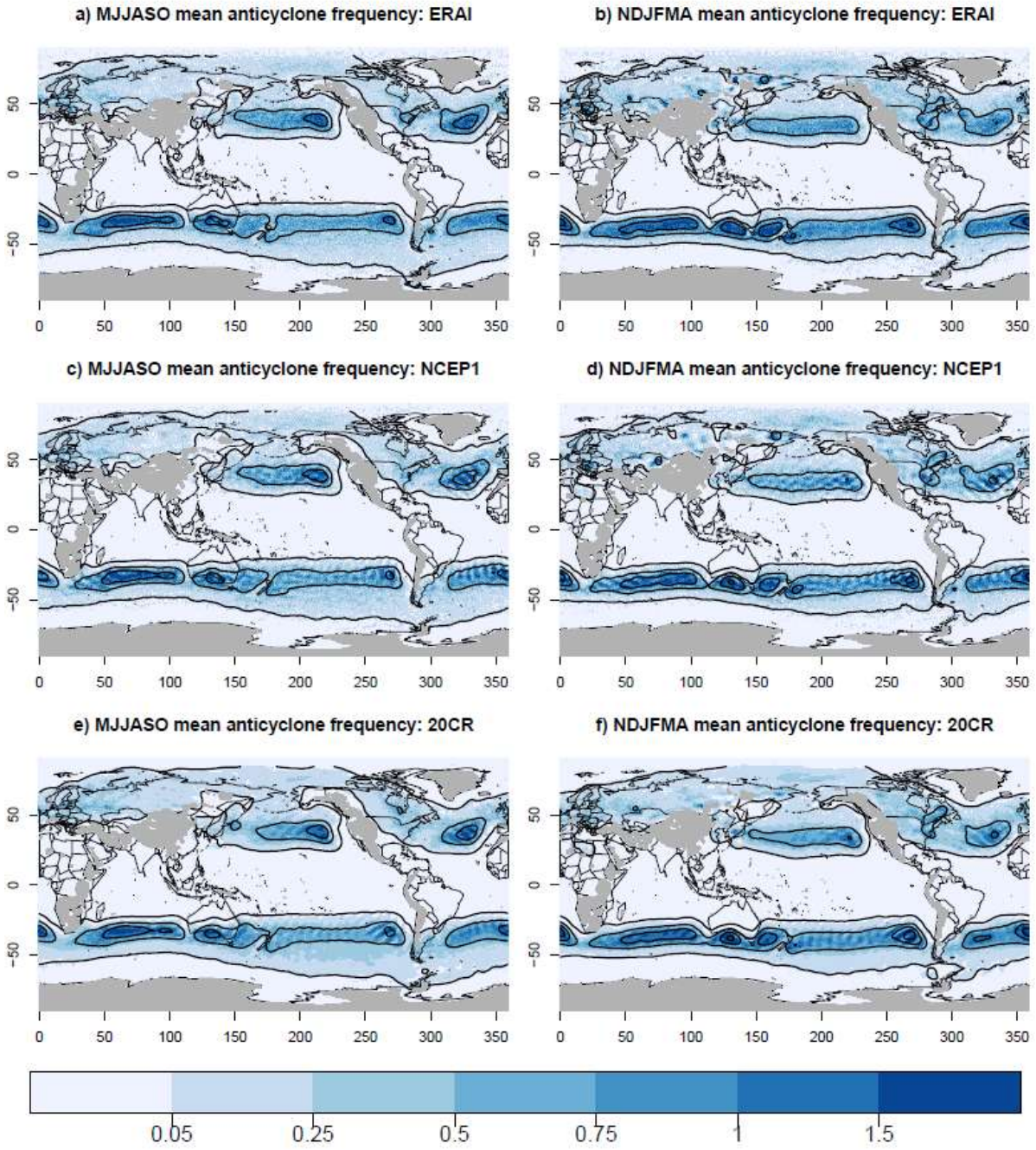

Figure 1. Average frequency of anticyclones (centres (deg. lat.)$^{-2}$) in May-October (left) and November-April (right) for three global reanalyses between 1980 and 2016: ERAI (top), NCEP1 (middle) and 20CR (bottom). Solid contours show frequencies of 0.05, 0.5, 1 and 1.5 centres (deg. lat.)$^{-2}$ using a 5° averaging window. Grey areas indicate topography higher than 1000 m in the ERA-Interim reanalysis, where anticyclones are not identified.

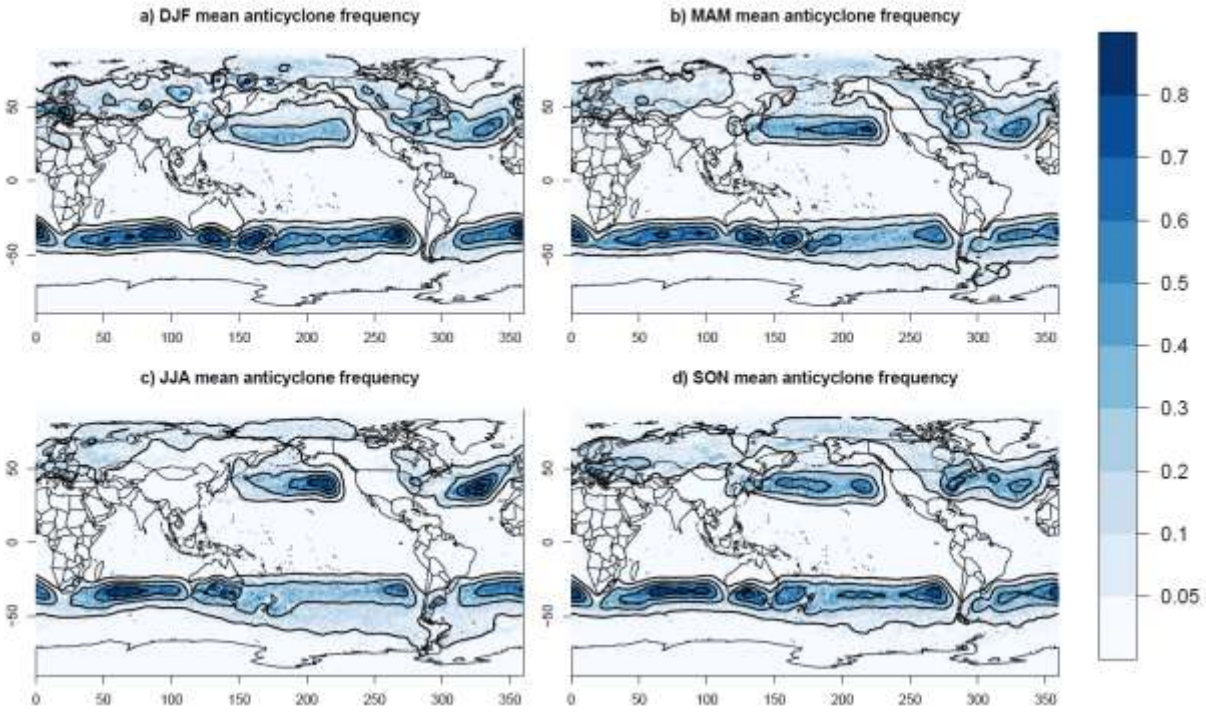

Figure 2. Average frequency of anticyclones (centres (deg. lat.)$^{-2}$) in ERAI for a) DJF, b) MAM, c) JJA and d) SON. Solid contours show frequency using a 5° averaging window, using every second contour (i.e. values of 0.05, 0.2, 0.4, 0.6 and 0.8).

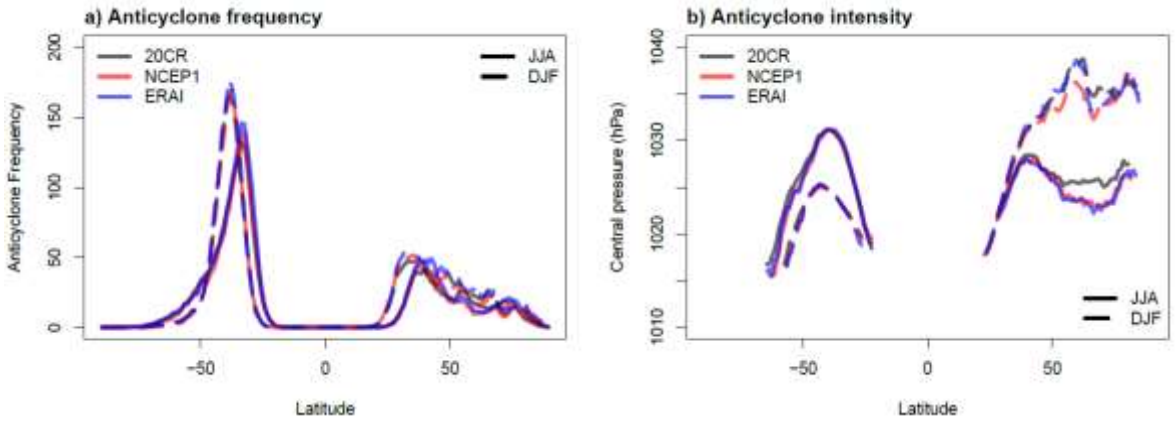

Figure 3. Average a) frequency and b) intensity (central pressure) of anticyclones by latitude, 1980-2014. Results are shown for ERAI, NCEP1, and the mean of 56 20CR ensemble members and split into the December-February and June-August seasons, with intensity only shown for latitudes where at least five anticyclone centres are observed per year.

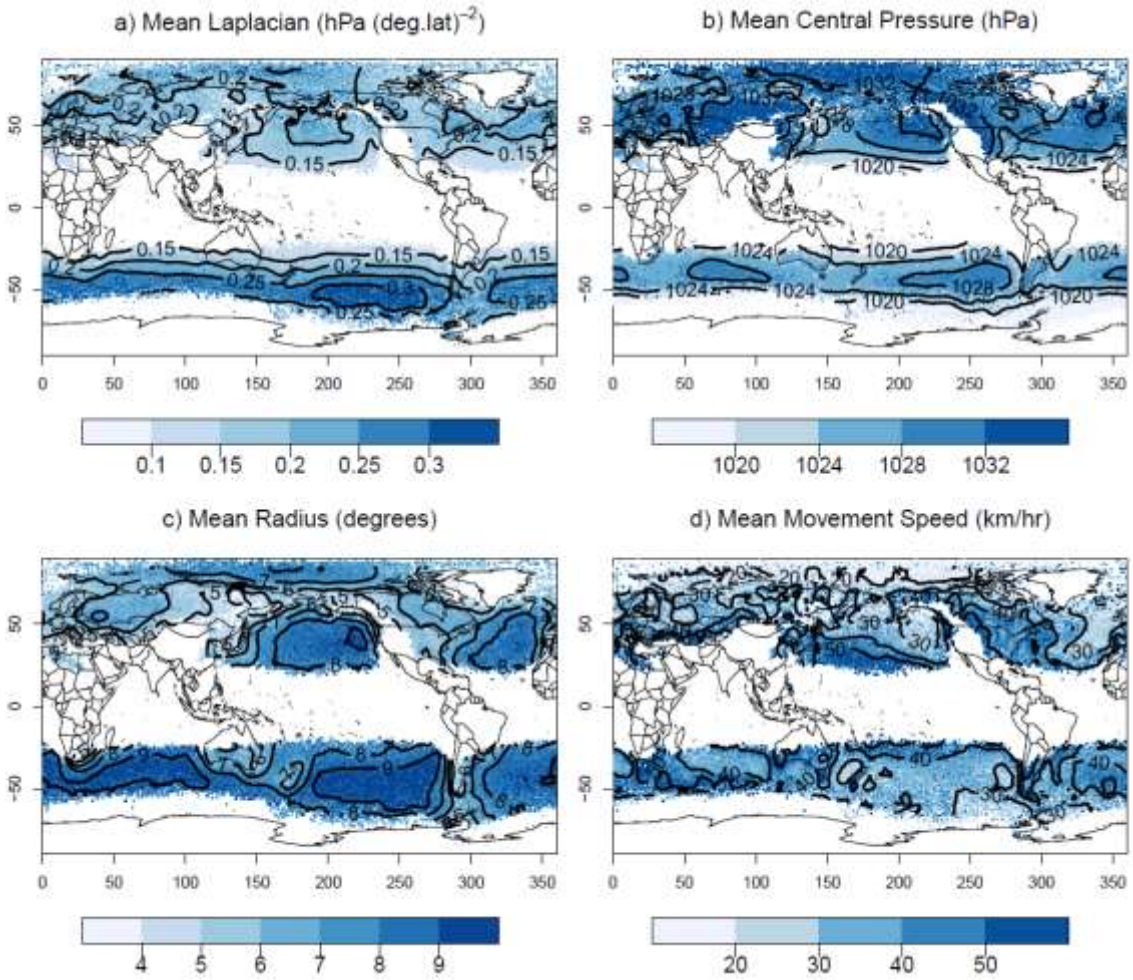

Figure 4. Average a) intensity (Laplacian), b) central pressure, c) radius and d) movement speed over the previous six hours for all anticyclones in ERAI, 1980-2016. Solid lines show smoothed data using a 5° averaging window. Values are only shown where the average anticyclone frequency is higher than 0.1 anticyclones/year.

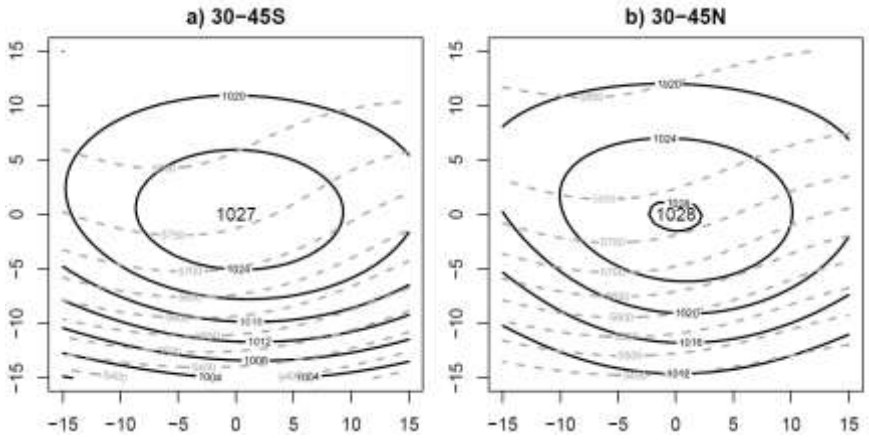

Figure 5. Composite mean sea level pressure (hPa, black) and 500 hPa geopotential height (m, grey) around anticyclones in the ERAI reanalysis, 1980-2016. Composites are shown within ± 15 degrees of latitude/longitude for anticyclones with centres located between a) 30-45°S and b) 30-45°N, and oriented so negative latitudes indicate poleward of the anticyclone centre.

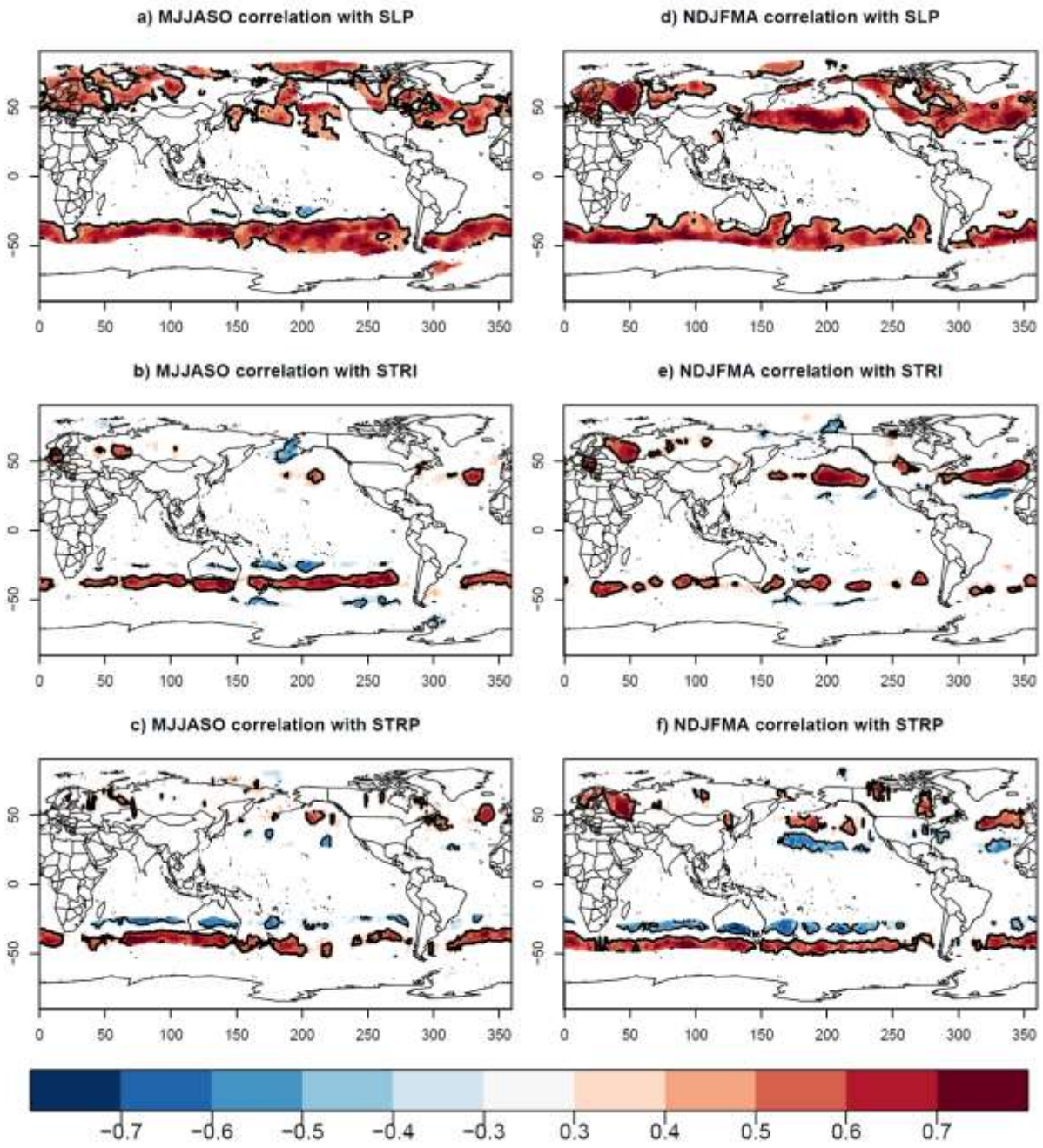

Figure 6. Correlation between anticyclone frequency in the ERA-Interim reanalysis between 1980 and 2016 in May-October (left) and November-April (right) with ERAI mean sea level pressure (top) and the intensity (centre) and position (bottom) of the subtropical ridge calculated for each longitude from ERAI. Correlations are calculated using anticyclone frequency smoothed over a 5° window and only shown where the correlation is locally significant (|r|>=0.325) and the average frequency is higher than 0.1 anticyclones/year. Solid lines show where the correlation is statistically significant at the 5% level after accounting for the false discovery rate, with thicker lines indicating positive correlations.

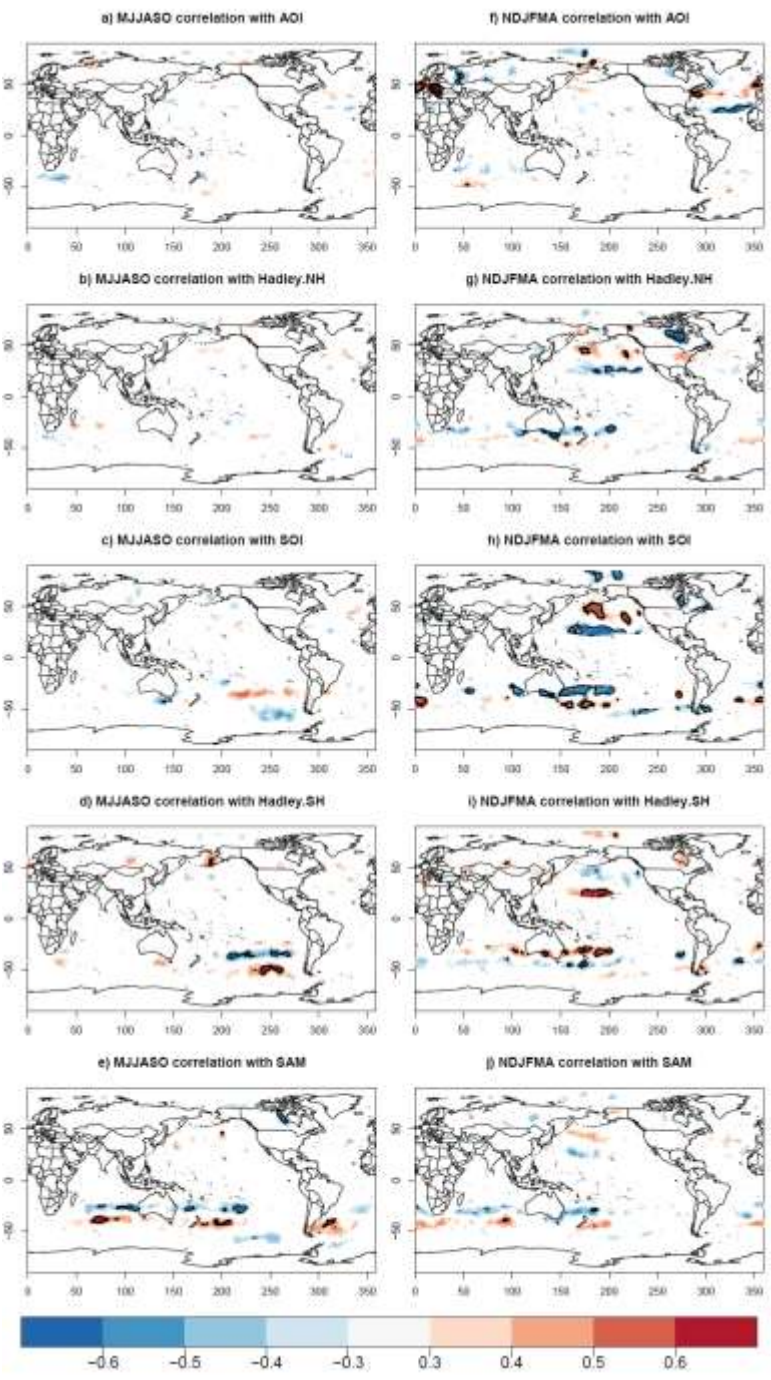

Figure 7. Correlation between anticyclone frequency in the ERA-Interim reanalysis between 1980 and 2016 in May-October (left) and November-April (right) with five indices of climate variability: the Arctic Oscillation, the latitude of the edge of the Hadley Cell in the Southern and Northern Hemispheres, the El Niño-Southern Oscillation (SOI) and the Southern Annular Mode. Correlations are calculated using anticyclone frequency smoothed over a 5° window and only shown where the correlation is locally significant (|r|>=0.325) and the average frequency is higher than 0.1 anticyclones/year. Solid lines show where the correlation is statistically significant at the 5% level after accounting for the false discovery rate, with thicker lines indicating positive correlations.

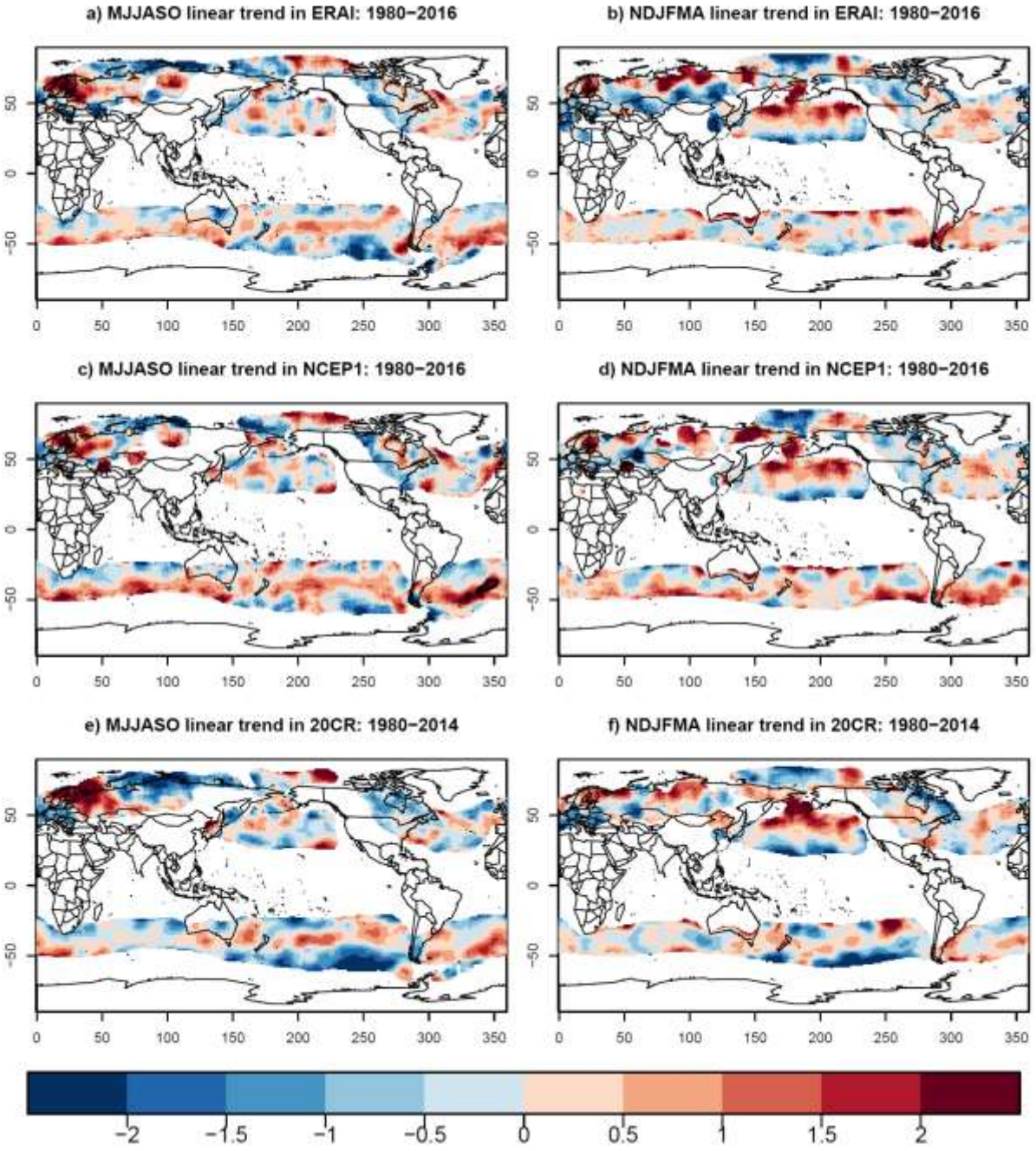

Figure 8. Linear trend in anticyclone centres per square degree between 1980 and 2016 in May-October (left) and November-April (right) for three global reanalyses: ERAI (top), NCEP1 (middle) and 20CR (bottom). Trends are shown as a percentage of the 1980-2016 mean frequency per year, and solid lines show where the trend is statistically significant at the 5% level after accounting for the false discovery rate, with thicker lines indicating positive correlations. Trends are only shown where the average frequency is higher than 0.1 anticyclones/year.

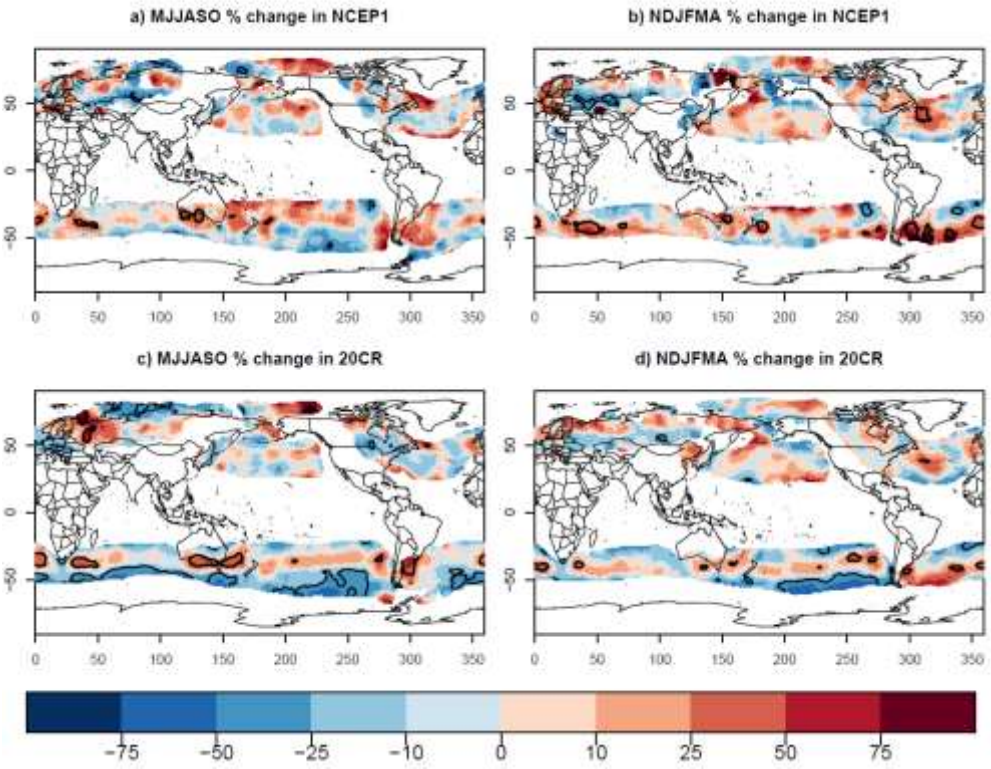

Figure 9. Percentage change in anticyclone centres per square degree between 1960-1979 and 1997-2016 in May-October (left) and November-April (right) for NCEP1 (top) and between 1960-1979 and 1997-2014 for 20CR (bottom). Solid lines show where the trend is statistically significant at the 5% level using a t-test after accounting for the false discovery rate, with thicker lines indicating positive correlations. Trends are only shown where the average frequency is higher than 0.1 anticyclones/year.

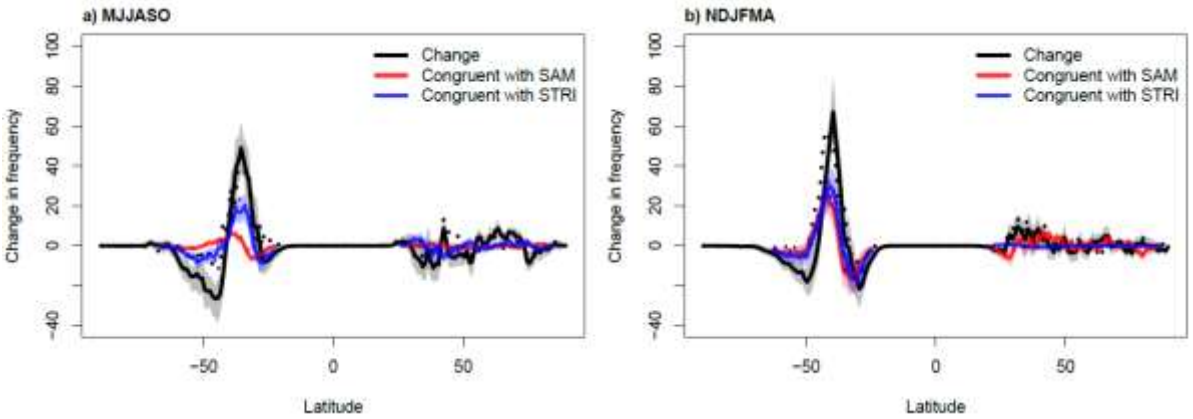

Figure 10. Change in the frequency of anticyclone centres by latitude for a) May-October and b) November-April and between 1960-1979 and 1997-2016. Shading indicates the range across the 56 20CR ensemble members with the solid lines indicating the ensemble mean, while dotted lines show the NCEP reanalysis. The trends congruent with trends in the Marshall (2003) SAM index and the hemispheric subtropical ridge intensity are also shown, based on recreated anticyclone frequencies from the observed relationship with the index over the 1960-2016 period.